Acoustic tethering of microorganisms

Rode, M.; Bioue, A.; Miano, F.; Bruus, H.; Kiørboe, T.; Andersen, A.

Published in:
Journal of Experimental Biology

Link to article, DOI:
10.1242/jeb.244089

Publication date:
2022

Document Version
Peer reviewed version

© 2019. MANUSCRIPT SUBMITTED TO JOURNAL OF EXPERIMENTAL BIOLOGY (2019) 00, jebxxxxxx. doi:10.1242/jeb.xxxxxx

METHODS & TECHNIQUES

Acoustic Tethering of Microorganisms

M. Rode[1], A. Bioue[2], F. Miano[1], H. Bruus[2], T. Kiørboe[1] and A. Andersen[1]

ABSTRACT

We show how to construct and apply a setup to acoustically tether and enable behavioral observations of individual microorganisms using simple laboratory equipment and a standard light microscope. We explore the capability of the setup with the freely swimming dinoflagellate *Alexandrium minutum* as study organism. We demonstrate that the setup allows us to tether cells in focus in the mid-plane of the sample chamber and make observations of individual organisms at high magnification without affecting their flagellar beat frequencies. We discuss the prospect of the method to explore appendage motion and swimming kinematics of other flagellates and ciliates.

KEYWORDS: Ultrasound, Video-Microscopy, Dinoflagellates

INTRODUCTION

Freely swimming microorganisms move as they please, and it requires patience to observe their appendage motions, swimming kinematics, and the resulting flows. To make a well-focused video recording, the experimentalist has to wait until the microorganism is swimming with a suitable orientation in the focus plane of the microscope, and a successful recording is not guaranteed. Here, we demonstrate the possibility to use ultrasound to tether freely swimming flagellates in the focus plane and enable easy observation of the behavior of individual microorganisms with simple laboratory equipment and a standard light microscope.

Observations and models of flagellar motion and propulsion have a long history (Gray, 1955; Gray and Hancock, 1955), and the fluid dynamics of swimming and feeding at the micro-scale continues to be an active research field (Guasto et al., 2012; Lauga, 2020). Three-dimensional swimming motions have been tracked using multiple, synchronized cameras (Drescher et al., 2009) and microscopes with automatic feedback-control to retain the individuals in focus (Berg, 1971; Darnige et al., 2017). Furthermore, observations of freely swimming flagellates have been carried out in three-dimensional chambers using standard microscopes (Drescher et al., 2010; Dölger et al., 2017), and detailed, time-resolved measurements have been made by confinement in quasi-two-dimensional water films (Guasto et al., 2010) and tethering using micropipettes (Brumley et al., 2014; Wei et al., 2019).

Contact-free, acoustic tethering is potentially an alternative to direct mechanical confinement and tethering. The use of ultrasound to manipulate small, suspended particles in a liquid is known as acoustofluidics, and it has over the past 20 years found widespread application to handle and separate particles and cells in microfluidic devices (Laurell et al., 2007). Acoustic tethering of micro-swimmers has been demonstrated for bacteria (Gutiérrez-Ramos et al., 2018), flagellates (Saito et al., 2002; Saito and Morita, 2006; Kim et al., 2019; 2021), ciliates (Saito et al., 1997; 2002), small multicellular worms (Baasch et al., 2018), and artificial, self-propelled particles (Takatori et al., 2016). These studies focused on tethering of populations of many individuals, e.g., to explore the properties of active suspensions (Takatori et al., 2016; Gutiérrez-Ramos et al., 2018), and as a tool to assess the swimming motility of *Chlamydomonas reinhardtii* by first confining and subsequently releasing a suspension of many flagellates (Kim et al., 2019).

Our aim in the following is to show how to construct and apply a simple setup to acoustically tether micro-swimmers and enable behavioral observations of individuals at high magnification. As far as we are aware, acoustic tethering has not been used previously for such observations, and the work on populations of many individuals by Gutierrez-Ramos et al. (2018) is the only study in which ultrasound has been used to tether micro-swimmers in the focus plane of the microscope. In the principle design, standing ultrasound waves in the MHz regime are generated in the water sample by a piezoelectric actuator (Fig. 1A), and freely swimming microorganisms are pushed to the mid-plane of the sample chamber and tethered by the acoustic radiation force that results when the ultrasound impinges on the organisms (Fig. 1B, C). We first describe the basic theory of ultrasound resonance and the acoustic radiation force on a small particle. Guided by the theoretical constraints, we present a design made of simple components that are easy to mount in a standard microscope. We demonstrate the tethering capability of the setup using the dinoflagellate *Alexandrium minutum*, and we explore the effect of ultrasound on its swimming and flagellar beat. We conclude by discussing the prospect of the method to explore other species of small aquatic organisms.

[1]Centre for Ocean Life, National Institute of Aquatic Resources, Technical University of Denmark, DK-2800 Kgs. Lyngby, Denmark
[2]Department of Physics, Technical University of Denmark, DK-2800 Kgs. Lyngby, Denmark

Authors for correspondence: (aanders@aqua.dtu.dk)

Date: 26 September 2022

Journal of Experimental Biology (2019) 00, jebxxxxxx. doi:10.1242/jeb.xxxxxx

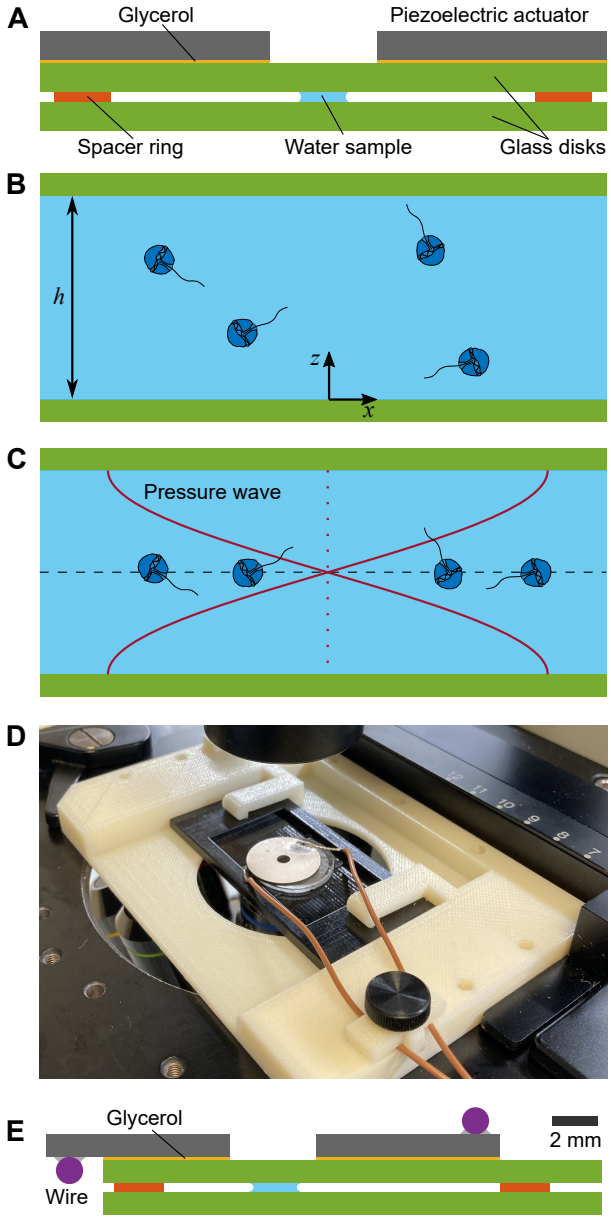

Fig. 1. The acoustic tethering principle and the experimental setup. (A) Schematic cross-section of the principle design to tether microorganisms using ultrasound. (B) Suspended microorganisms (circles, dark blue) swim freely in the absence of ultrasound. (C) A standing sound wave is formed in the water sample due to the vibrations of the piezoelectric actuator, and the resulting acoustic radiation force tethers the organisms in the nodal mid–plane (dashed line, black) of the pressure wave (solid lines, red) between the plates of the sample chamber. (D) The sample chamber with the ring-shaped actuator in the inverted microscope. The actuator was driven by a sinusoidal voltage signal supplied by a frequency generator via the pair of wires. (E) Schematic cross-section of the sample chamber in the experimental setup with wires (purple) and solder (light grey). The two glass disks were concentric, whereas the water sample, the spacer ring, and the actuator were displaced off center in the cross-sectional plane to accommodate the wire on the lower face of the actuator. The schematic is to scale.

MATERIALS AND METHODS

Ultrasound resonance

Sound waves in water are time-varying perturbations of density ρ, pressure p, and velocity $\vec{v}$ relative to a quiescent equilibrium state with constant density ρ_0, pressure p_0, and velocity $\vec{v}_0 = \vec{0}$. We use the subscript "1" to denote the perturbations, so that $\rho = \rho_0 + \rho_1$, $p = p_0 + p_1$, and $\vec{v} = \vec{v}_1$. When the perturbations are small, the governing equations are the linearised, inviscid equations for a compressible fluid, i.e., the Euler equation, the equation of continuity, and the isentropic equation of state:

$$\rho_0 \, \partial_t \vec{v}_1 = -\vec{\nabla} p_1 \,, \tag{1}$$

$$\partial_t \rho_1 = -\rho_0 \vec{\nabla} \cdot \vec{v}_1 \,, \tag{2}$$

$$p_1 = \frac{1}{\rho_0 \, \kappa_0} \rho_1 \,, \tag{3}$$

where κ_0 is the compressibility (Lighthill, 1978). The equations can be combined to form the linear wave equation:

$$\partial_t^2 p_1 = c_0^2 \, \nabla^2 p_1 \,, \tag{4}$$

where $c_0 = (\rho_0 \, \kappa_0)^{-1/2}$ is the speed of sound. The basic ultrasound resonance is the fundamental plane wave solution in the water-filled gap between two infinite, parallel and rigid plates:

$$p_1 = A \cos\left(\frac{\pi \, z}{h}\right) \sin\left(2 \, \pi \, f \, t\right) \,, \tag{5}$$

$$\vec{v}_1 = -\frac{A}{\rho_0 \, c_0} \sin\left(\frac{\pi \, z}{h}\right) \cos\left(2 \, \pi \, f \, t\right) \vec{e}_z \,, \tag{6}$$

where f is the frequency of the wave and A the amplitude of the pressure wave (Bruus, 2012a). The wavelength λ is twice the gap height h, the z-direction is normal to the plates, and the plates are positioned at $z = 0$ and $z = h$ (Fig. 1B). The pressure wave has a nodal plane in the middle of the gap (Fig. 1C), since we assume that the plates have hard-wall boundary condition in which the normal velocity component is zero. From the wave relation $c_0 = \lambda \, f$, we obtain the important design condition:

$$c_0 = 2 \, h \, f \,, \tag{7}$$

since $\lambda = 2 \, h$ in the fundamental mode. This condition constrains the choice of the piezoelectric actuator.

The acoustic radiation force on a small particle

A suspended particle scatters sound waves and experiences an acoustic radiation force if its compressibility and density differ from those of the water (Gorkov, 1962). The acoustic radiation force on a small, spherical particle in the basic ultrasound wave resonance can be written (Bruus, 2012b):

$$\vec{F} = -\frac{4}{3} \, \pi \, a^3 \, \vec{\nabla} \left[\alpha \left(\kappa_\mathrm{p} - \kappa_0\right) \left\langle p_1^2 \right\rangle + \beta \left(\rho_\mathrm{p} - \rho_0\right) \left\langle v_1^2 \right\rangle \right] \,, \tag{8}$$

where a is the radius of the particle, κ_p and ρ_p its compressibility and density, respectively, and α and β the two coefficients:

$$\alpha = -\frac{1}{2} \,, \qquad \beta = -\frac{3\rho_0}{4\rho_\mathrm{p} + 2\rho_0} \,. \tag{9}$$

The expression is to be evaluated at the position of the particle, and it is assumed that $a \ll \lambda$. The symbol $\langle \cdots \rangle$ denotes the time

average over one full period, and for the wave in Eqns 5 and 6 we find:

$$\left\langle p_1^2 \right\rangle = \frac{1}{2} A^2 \cos^2\left(\frac{\pi z}{h}\right) , \quad (10)$$

$$\left\langle v_1^2 \right\rangle = \frac{1}{2}\left(\frac{A}{\rho_0 c_0}\right)^2 \sin^2\left(\frac{\pi z}{h}\right) . \quad (11)$$

The force vanishes if $\kappa_\mathrm{p} = \kappa_0$ and $\rho_\mathrm{p} = \rho_0$, and it is proportional to the volume of the particle. By inserting Eqns 10 and 11 in Eqn 8 and evaluating the expression, we find the acoustic radiation force:

$$\vec{F} = \frac{4\pi^2 a^3 \Phi E}{3h} \sin\left(\frac{2\pi z}{h}\right) \vec{e}_z , \quad (12)$$

where Φ is the acoustophoretic contrast factor:

$$\Phi = \frac{5\rho_\mathrm{p} - 2\rho_0}{2\rho_\mathrm{p} + \rho_0} - \frac{\kappa_\mathrm{p}}{\kappa_0} , \quad (13)$$

and E the acoustic energy density:

$$E = \frac{1}{4}\kappa_0 A^2 . \quad (14)$$

The sign of the acoustophoretic contrast factor determines the qualitative effect of the acoustic radiation force (Bruus, 2012b). Heavy and hard particles with $\Phi > 0$ are pushed towards the pressure node in the mid-plane (Fig. 1C), whereas light and soft particles with $\Phi < 0$ are pushed towards the pressure antinodes at the walls. The force is proportional to the acoustic energy density which results as a balance between the piezoelectric actuation and the dissipation in the system. The acoustic energy density is proportional to the square of the amplitude of the sinusoidal voltage signal driving the piezoelectric actuator (Barnkob et al., 2010), and the magnitude of the acoustic radiation force can therefore be adjusted directly in the experiment.

The characteristic value of the acoustic radiation force

To estimate the characteristic value of the acoustic radiation force in the experiment, we can use the observed time scale for the motion of the microorganisms to the mid-plane when the ultrasound is turned on. As a simple model of the dynamics, we assume that the acoustic radiation force in Eqn 12 is balanced by the Stokes drag on the cell body of the microorganism:

$$6\pi\mu a \frac{\mathrm{d}z}{\mathrm{d}t} = F_0 \sin\left(\frac{2\pi z}{h}\right) , \quad (15)$$

where μ denotes the viscosity and F_0 the characteristic value of the acoustic radiation force:

$$F_0 = \frac{4\pi^2 a^3 \Phi E}{3h} . \quad (16)$$

In the model, we disregard the swimming apparatus of the microorganism and assume that it can be modeled as a passive, spherical particle. The governing equation can be integrated analytically (Barnkob et al., 2010), and this allows us to estimate F_0 directly from the experimentally observed trajectories:

$$F_0 = \frac{3\mu a h}{\tau} \ln\left[\frac{\tan(\pi z_\mathrm{f}/h)}{\tan(\pi z_\mathrm{i}/h)}\right] , \quad (17)$$

where τ is the time that it takes for a microorganism to be pushed from its initial position z_i to its final position z_f. The acoustic radiation force vanishes in the mid-plane and on the lower and the upper boundary of the sample chamber, and with $\Phi > 0$ we will have either $0 < z_\mathrm{i} < z_\mathrm{f} < h/2$ or $h > z_\mathrm{i} > z_\mathrm{f} > h/2$.

Design requirements

Standard seawater with salinity $35\,\mathrm{g\,kg^{-1}}$ at atmospheric pressure and $20\,^\circ\mathrm{C}$ has $\rho_0 = 1025\,\mathrm{kg\,m^{-3}}$, $\kappa_0 = 4.28\times10^{-10}\,\mathrm{Pa^{-1}}$, and $c_0 = 1522\,\mathrm{m\,s^{-1}}$ (Kaye and Laby, 1995). It follows from Eqn 7 that a piezoelectric actuator driven at the frequency $f = 2.0\,\mathrm{MHz}$ can excite the fundamental mode between two parallel plates with $h = 0.38\,\mathrm{mm}$. For a typical cell with $\rho_\mathrm{p} = 1100\,\mathrm{kg\,m^{-3}}$ and $\kappa_\mathrm{p} = 4.00\times10^{-10}\,\mathrm{Pa^{-1}}$ (Bruus, 2012c), we find $\Phi = 0.135$ using Eqn 13, and the positive acoustophoretic contrast factor suggests that the cell will be pushed towards the mid-plane and tethered as discussed above. A list of more precise values of the density and the compressibility of various cells can be found in Cushing et al. (2017).

Study organisms

We used the dinoflagellate *Alexandrium minutum* as a representative microorganism to characterize the tethering capability of the setup (Fig. 1B). The phototrophic dinoflagellate swims using a transverse flagellum situated in a groove encircling the cell body and a longitudinal flagellum trailing the cell body (Fenchel, 2001; Lewis et al., 2006). The cell culture was maintained in filtered seawater with added B1 medium at $18\,^\circ\mathrm{C}$ (Hansen, 1989), and the culture was diluted once every month.

Furthermore, we worked with the ciliate *Euplotes vannus* to demonstrate the capability of the setup to tether relatively large microorganisms. The heterotrophic ciliate feeds on suspended food particles using a membranellar band that consists of rows of closely spaced cilia (Fenchel, 1980; Rode et al., 2022). The cell culture was grown in artificial seawater at $18\,^\circ\mathrm{C}$ and diluted 2-3 times per year with artificial seawater and autoclaved rice grains to serve as bacterial substrate (Rode et al., 2022).

Experimental setup and method

The design of the experimental setup was aided by three-dimensional simulations building on Eqns 1, 2, 3, 8, and 9, and using models of the glass disks, spacer ring, and piezoelectric actuator following the numerical method developed by Skov et al. (2019). The method was implemented in the finite-element software COMSOL using the mathematics-weakform-PDE module as exemplified by the scripts provided in the Supplemental Material of Muller and Bruus (2015). In the final design (Fig. 1D), the sample chamber was made of two disks and a spacer ring enclosing the

water sample with suspended microorganisms (Fig. 1E). The two circular glass disks of thickness $1\,\mathrm{mm}$ and diameter $22\,\mathrm{mm}$ were made from standard microscope slides (soda-lime glass) using a water jet cutting machine. Preliminary experiments were made with standard coverslips of thickness $0.170\,\mathrm{mm}$ and $0.300\,\mathrm{mm}$, but the coverslips turned out to be too thin to allow efficient excitation of the fundamental mode, and the preliminary experiments were unsuccessful. The spacer ring was made from a rubber-like aerobic resistance band with a thickness of $h = 0.38\,\mathrm{mm}$, and a Young's modulus and a Poisson's ratio of roughly $1\,\mathrm{MPa}$ and 0.5, respectively. The thickness of the spacer ring was selected to allow the fundamental mode at the frequency $f = 2.0\,\mathrm{MHz}$ as discussed above. The spacer ring was cut with a custom-made die with an inner diameter of $15\,\mathrm{mm}$ and an outer diameter of $19\,\mathrm{mm}$. The smooth rubber-like surface provided strong and stable contact with the two glass disks, and it effectively sealed the sample chamber from the ambient air.

The piezoelectric actuator was attached on top of the upper glass disk by a thin layer of glycerol with a thickness of roughly $1\,\mu\mathrm{m}$ (Fig. 1E). Glycerol is commonly used as coupling layer in acoustofluidics (Hammarström et al., 2010; Lenshof et al., 2012; Lickert et al., 2021), and it allows for the setup to be easily assembled and disassembled. The ring-shaped actuator with an inner diameter of $3.8\,\mathrm{mm}$, an outer diameter of $20\,\mathrm{mm}$, and a thickness of $1\,\mathrm{mm}$ is a standard component made of the material Pz26 and designed to resonate at $2.0\,\mathrm{MHz}$ (Meggitt A/S, Kvistgård, Denmark). The geometry of the sample chamber and the central hole in the actuator made it easy to illuminate the water sample from above and observe it from below in the inverted microscope (Fig. 1D). The flat faces of the actuator were coated with silver electrodes, and a wire was soldered onto each face (Fig. 1E). The wires were placed close to the outer rim of the actuator, and the actuator was positioned slightly off center to establish a good coupling between its lower face and the upper glass disk. The function of the setup was robust and not sensitive to the details of the off-center placement of the actuator. The actuator was driven by a sinusoidal voltage signal from a function generator (Keysight Technologies 33522B Series Waveform Generator).

The sample chamber was assembled in each new experiment. First, the spacer ring was positioned directly on the lower glass disk, and the water sample with suspended microorganisms was placed centrally inside the spacer ring using a microliter pipette (LABSOLUTE, Th. Geyer GmbH & Co. KG). Subsequently, the upper glass disk was placed directly on top of the spacer ring (Fig. 1E). Depending on its volume, the sample either fills the sample chamber or forms a rotationally symmetric capillary bridge between the two glass plates (Fortes, 1982). Finally, the piezoelectric actuator was positioned on top of the upper glass disk with a thin coupling layer of glycerol. Throughout observations, we used a sample chamber holder (black) and an adapter (white) for the microscope stage table (Fig. 1D). The two components were 3D printed with the designs provided in Supplementary Materials and Methods. In the idealized, one-dimensional model, we have Eqn 7, and the gap height $h = 0.38\,\mathrm{mm}$ corresponds to the fundamental resonance frequency $f = 2.0\,\mathrm{MHz}$. In practice, and as also studied in our numerical simulations, the modes are three-dimensional, and the resonance spectrum varies across sample chamber assemblies and contains around the fundamental resonance frequency a handful of modes with a nodal mid-plane. In each experiment, it is therefore necessary to search for a good resonance. This is done by observing the sample in the microscope while varying the frequency of the voltage signal around $2\,\mathrm{MHz}$ in steps of $10\,\mathrm{kHz}$ until a frequency is found at which the suspended organisms are pushed rapidly into focus in the mid-plane of the sample chamber. Alternatively, one can excite all resonances in a range around the fundamental resonance frequency by varying the frequency of the voltage signal, e.g., in the frequency range $1.95 - 2.05\,\mathrm{MHz}$ using a triangular sweep with repetition frequency $0.5\,\mathrm{kHz}$ (Manneberg et al., 2009).

Video observations and data analysis

We used an Olympus IX71 inverted microscope and a Phantom Miro LAB 320 high-speed video camera (1920×1200 pixels) at $10\times$ magnification (Olympus UPlanFL, working distance $10\,\mathrm{mm}$) and a frame rate of 25 fps to observe the swimming trajectories of *A. minutum* and $40\times$ magnification (Olympus LCPlanFL, working distance $2.15 - 2.89\,\mathrm{mm}$) and a frame rate of 1000 fps to see the flagellar beat of *A. minutum* and the membranelle motion of *E. vannus*. The observations were made in a temperature-controlled room at $20^{\circ}\mathrm{C}$. The dinoflagellates were tracked automatically using custom-written code. Our script in MATLAB and a series of video frames to illustrate the use of the code can be downloaded from the data repository DTU Data. To explore the effect of the acoustic tethering on the beat frequency of the longitudinal flagellum of *A. minutum*, we considered a sample of nine different individuals. For each individual we visually inspected high-speed video of 15 uncorrelated beats before and 15 uncorrelated beats after the ultrasound was turned off and determined the mean and the standard deviation of the mean of the beat frequencies f_{on} and f_{off} with and without ultrasound, respectively.

RESULTS AND DISCUSSION

Tethering of freely swimming dinoflagellates

To illustrate the tethering capability of the setup, we present an experiment with three freely swimming individuals of *A. minutum* (Video 1). The $1\,\mu\mathrm{L}$ water sample formed a capillary bridge with an inner diameter of $1.4\,\mathrm{mm}$ between the two glass disks, and the piezoelectric actuator was driven by a sinusoidal voltage signal with frequency $1.97\,\mathrm{MHz}$ and peak-to-peak amplitude $20\,\mathrm{V}$ (high-impedance output). We focus on one of the three individuals to explore the swimming motion and the tethering quantitatively (Fig. 2). Initially, the individual with diameter $18\,\mu\mathrm{m}$ was not swimming in the focus plane of the microscope (Fig. 2A). The ultrasound was turned on at time zero, and the organism was

Journal of Experimental Biology (2019) 00, jebxxxxxx. doi:10.1242/jeb.xxxxxx

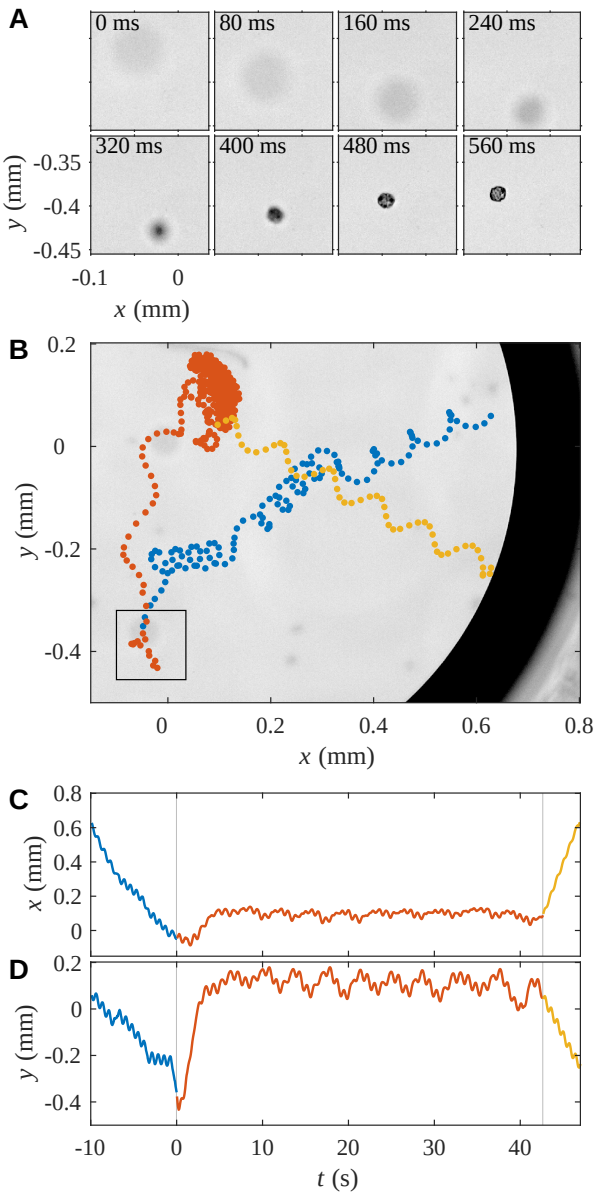

Fig. 2. Swimming dinoflagellate in the sample chamber with and without ultrasound. (A) Video sequence with $80\,\mathrm{ms}$ between consecutive frames and the first frame showing the instant when the ultrasound was turned on. Initially, the cell was out of focus, and it was gradually forced into focus in the mid-plane. (B) - (D) Swimming trajectory (two-dimensional projection) before time zero when the ultrasound was turned on (blue), while the ultrasound was on (orange), and after the ultrasound was turned off again (yellow). There is $80\,\mathrm{ms}$ between consecutive dots in (B). The vertical lines in (C) - (D) indicate the transitions when the voltage signal with frequency $1.97\,\mathrm{MHz}$ and peak–to-peak amplitude $20\,\mathrm{V}$ was turned on and off, respectively. The field of view in (A) is indicated by the square box in (B) that shows the frame at time zero, and the circular rim (black) of the capillary bridge is visible in (B).

brought into focus in the mid-plane after $480 - 560\,\mathrm{ms}$. Subsequently, the organism swam in the mid-plane, and it was ultimately confined in a small area of approximately $100\,\mu\mathrm{m} \times 150\,\mu\mathrm{m}$ in the central part of the capillary bridge (Fig. 2B-D). The extent of the lateral confinement depends on the specific assembly of the setup and the details of the acoustic radiation force in the three-dimensional resonance.

After the ultrasound was turned off again, the individual swam freely with a helical trajectory with the central axis approximately in the mid-plane. Helical swimming trajectories are typical for dinoflagellates and many other microorganisms (Purcell, 1977; Fenchel, 2001). Assuming a simple helical trajectory with the central axis in the xy-plane (Crenshaw, 1993), we find the radius $22\,\mu\mathrm{m}$, the pitch $110\,\mu\mathrm{m}$, and the frequency $1.4\,\mathrm{Hz}$. The parameters correspond to the swimming speed $240\,\mu\mathrm{m\,s^{-1}}$, which is normal for individuals of *A. minutum* (Lewis et al., 2006).

To estimate the thrust, T, produced by the flagella, we assume that it is equal in magnitude to the Stokes drag, D, on the cell body when the dinoflagellate is freely swimming:

$$T = D = 6\,\pi\,\mu\,a\,U\,, \tag{18}$$

where U is the swimming speed. With $\mu = 1\,\mathrm{mPa\,s}$, $a = 9\,\mu\mathrm{m}$, and $U = 240\,\mu\mathrm{m\,s^{-1}}$, we find the estimate: $T = 41\,\mathrm{pN}$. For comparison we can use Eqn 17 to estimate the characteristic value of the acoustic radiation force, and we find $F_0 = 73\,\mathrm{pN}$, where we have used $\tau = 520\,\mathrm{ms}$ and assumed that $z_\mathrm{i} = h/20$ and $z_\mathrm{f} = 9\,h/20$ (Fig. 2A). As expected, the estimate of the characteristic value of the acoustic radiation force is greater than the estimate of the thrust produced by the dinoflagellate.

The effect of ultrasound on swimming and flagellar beat

We expect the tethering capability to depend on the amplitude of the voltage signal driving the piezoelectric actuator as summarized in Eqns 12 - 14 and the subsequent discussion. We explored this effect in a sample with a few individuals of *A. minutum* subject to different voltage signals. In the experiment, the peak-to-peak amplitude, U, was reduced in a step-wise fashion as function of time (Fig. 3A), and we focused on a representative individual with cell diameter $20\,\mu\mathrm{m}$ (Fig. 3B-D). The cell was kept in focus and confined to a large, central area in the mid-plane at $U = 20\,\mathrm{V}$ and $U = 15\,\mathrm{V}$, whereas it was swimming more freely and out of the mid-plane at and below $U = 10\,\mathrm{V}$ (Fig. 3B, C). In the experiment, the cell first moved significantly out of focus at $U = 10\,\mathrm{V}$ as shown in the selected video sequence (Fig. 3D).

The ultrasound allows us to tether the dinoflagellates, but it could potentially affect the organisms in unwanted ways, e.g., by altering their flagellar beat frequencies. As a test, we determined the beat frequency of the longitudinal flagellum for several different individuals when the actuation with peak-to-peak amplitude $20\,\mathrm{V}$ was on and off, respectively (Video 2). The motion of the longitudinal flagellum is clearly observable, whereas the transverse flagellum and the rotation of the cell are difficult to follow. We therefore only report data for the beat frequency of the longitudinal flagellum. The individuals were released when the ultrasound was turned off, but they remained in focus for at least 30 consecutive beat periods which allowed us to determine the beat frequency

Journal of Experimental Biology (2019) 00, jebxxxxxx. doi:10.1242/jeb.xxxxxx

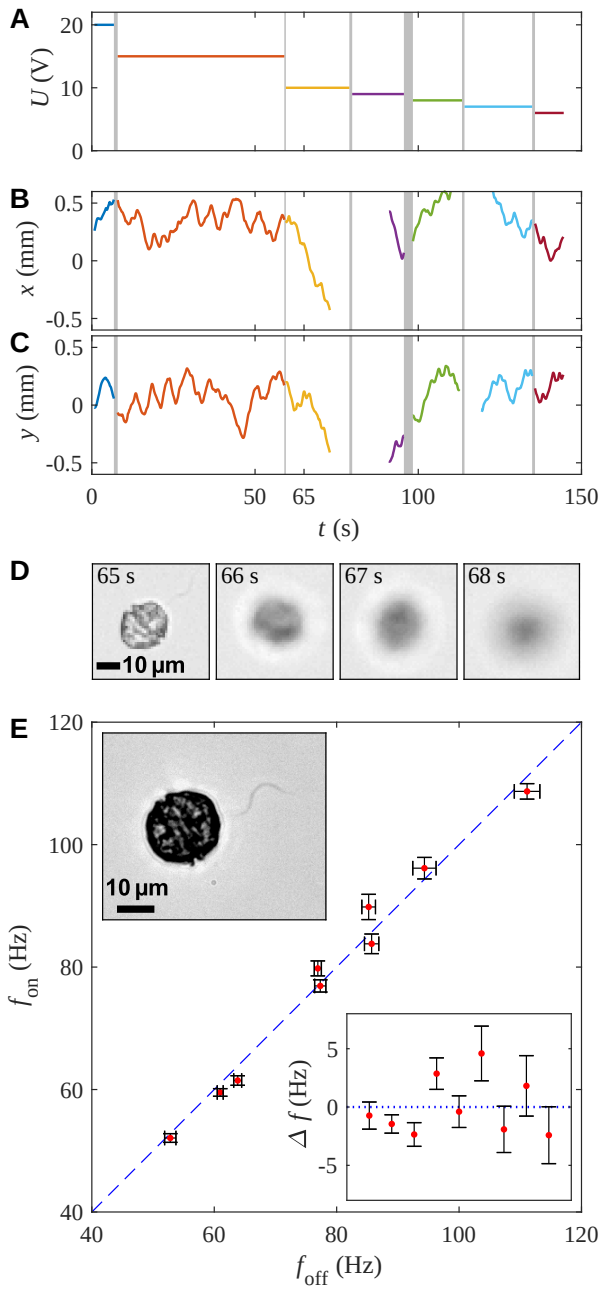

Fig. 3. The effect of ultrasound on the swimming and the flagellar beat frequency of the dinoflagellate. (A) The peak-to-peak amplitude of the voltage signal and (B) - (D) cell position and video frame sequence in an experiment where the voltage was decreased in a step-wise fashion. (B) - (C) Coordinates as functions of time and (D) frames when the cell first moved out of the focus plane. The vertical lines indicate the transitions between voltage levels, and there are gaps in the curves in (B) - (C) when the individual was in the dark rim of the capillary bridge. (E) The beat frequency of the longitudinal flagellum (upper inset) for nine individuals when the actuation was off and on, respectively. Each data point represents an individual, and the one–to-one relation (dashed line, blue) is shown as reference. The lower inset shows $\Delta f = f_{\mathrm{on}} - f_{\mathrm{off}}$ with zero (dotted line, blue) as reference, and the data points are ordered with increasing value of f_{off}. The data points are mean values, and the error bars show one standard deviation of the mean.

in the absence of ultrasound. There is large variability across individuals, but for each individual we find that f_{off} and f_{on} are similar (Fig. 3E). The frequency differences, $\Delta f = f_{\mathrm{on}} - f_{\mathrm{off}}$, are distributed around zero, and the average frequency difference of the nine individuals, $\overline{\Delta f} = 0.0005 \pm 0.8370\,\mathrm{Hz}$, is not statistically different from zero (t-test, p-value of 0.9996). (The uncertainty in $\overline{\Delta f}$ is shown as one standard deviation of the mean.) The result suggests that the method is sufficiently gentle to allow tethering without influencing the natural beat pattern.

Perspective

We have demonstrated that the setup allows us to tether and make behavioral observations of individual microorganisms using *A. minutum* as a study organism. Our result on the beat frequency of the longitudinal flagellum suggests that the flagellar apparatus is only weakly influenced by the ultrasound. We presume that the setup will work to confine other flagellates and ciliates. As a simple demonstration we have tethered the ciliate *E. vannus* with a cell length of roughly $90\,\mu\mathrm{m}$ (Video 3), and we are able to observe the beating of the cilia in the membranellar band (Fenchel, 1980; Rode et al., 2022). Tethering of even larger organisms should be possible by choosing a piezoelectric actuator with a lower resonance frequency and increasing the gap height according to Eqn 7, as long as the observations are not constrained by the working distance of the microscope objective.

The swimming speed and the beat frequency of a typical microorganism are on the order of $100\,\mu\mathrm{m\,s^{-1}}$ and $50\,\mathrm{Hz}$, respectively, and if we assume that the thickness of the focus plane of the microscope (depth of field) is $40\,\mu\mathrm{m}$ at high magnification, we estimate that a typical, freely swimming individual will remain in focus for roughly 20 beat periods. A possible use of the method is therefore to bring the microorganism into the focus plane and subsequently release and observe it freely swimming. This approach allows observations of short swimming sequences, and it cannot replace microscopes designed specifically to follow long, three-dimensional swimming trajectories (Berg, 1971; Drescher et al., 2009; Darnige et al., 2017).

The acoustic radiation force is proportional to the cell radius cubed (Eqn 8), and the force might not be sufficient to tether micron-sized bacteria and small flagellates. Instead, the motion of micron-sized organisms may be dominated by acoustic streaming caused by motion in the viscous boundary layers at the walls of the sample chamber (Bruus, 2012c) and in the bulk liquid by the slight heating from the actuator (Joergensen and Bruus, 2021). Optical tethering provides an alternative to acoustic tethering (Thalhammer et al., 2011; Dholakia et al., 2020), and it is particularly advantageous for tethering of particles and cells with size less than one micron (Dholakia et al., 2020).

Acoustic tethering is not limited to spherical cells as demonstrated for small multicellular worms (Baasch et al., 2018), but more work is needed to theoretically and experimentally understand the acoustic radiation force and torque on elongated cells and thin fibers like flagella and cilia (Leão-Neto et al., 2021).

Acknowledgements

We are grateful to Meggitt A/S for providing piezoelectric actuators, Kirstine Berg-Sørensen, Anders Nielsen, Lars Pedersen, Fredrik Ryderheim, Ole Trinhammer, and Willem van de Water for help and advice, and Erik Hansen for his careful work on design and construction of the experimental setup and for the technical drawings in Supplementary Materials and Methods. The results presented in Fig. 2 in this paper are reproduced from the PhD thesis of Mads Rode (Technical University of Denmark, 2021).

Competing interests

The authors declare no competing interests.

Contribution

M.R., H.B., T.K., and A.A. designed the research; M.R., A.B., and F.M. carried out the experiments; H.B. performed numerical simulations; and M.R. and A.A. wrote the paper. All authors commented on the paper.

Funding

This project received funding from The Independent Research Fund Denmark (grant no. 7014-00033B), the Centre for Ocean Life, a VKR Centre of Excellence supported by the Villum Foundation, the Carlsberg Foundation (grant no. CF17-0495), and the European Union's Horizon 2020 research and innovation programme under the Marie Skłodowska-Curie grant agreement No 955910.

Data availability

The MATLAB script with our particle tracking code and a series of video frames to which the MATLAB script can be applied is deposited in the data repository DTU Data (https://doi.org/10.11583/DTU.21206291). The beat frequency data shown in Fig. 3E are available upon request.

REFERENCES

Baasch, T., Reichert, P., Lakämper, S., Vertti-Quintero, N., Hack, G., Casadevall i Solvas, X., deMello, A., Gunawan, R. and Dual, J. (2018). Acoustic Compressibility of *Caenorhabditis elegans*. *Biophysical Journal* 115, 1817–1825.

Barnkob, R., Augustsson, P., Laurell, T. and Bruus, H. (2010). Measuring the local pressure amplitude in microchannel acoustophoresis. *Lab on a Chip* 10, 563–570.

Berg, H. C. (1971). How to track bacteria. *Rev. Sci. Instrum.* 42, 868–871.

Brumley, D. R., Wan, K. Y., Polin, M. and Goldstein, R. E. (2014). Flagellar synchronization through direct hydrodynamic interactions. *eLife* 3, e02750.

Bruus, H. (2012a). Acoustofluidics 2: Perturbation theory and ultrasound resonance modes. *Lab on a Chip* 12, 20–28.

Bruus, H. (2012b). Acoustofluidics 7: The acoustic radiation force on small particles. *Lab on a Chip* 12, 1014–1021.

Bruus, H. (2012c). Acoustofluidics 10: Scaling laws in acoustophoresis. *Lab on a Chip* 12, 1578–1586.

Crenshaw, H. C. (1993). Orientation by helical motion - I. Kinematics of the helical motion of organisms with up to six degrees of freedom. *Bulletin of Mathematical Biology* 55, 197–212.

Cushing, K. W., Garofalo, F., Magnusson, C., Ekblad, L., Bruss, H. and Laurell, T. (2017). Ultrasound Characterization of Microbead and Cell Suspensions by Speed of Sound Measurements of Neutrally Buoyant Samples. *Anal. Chem.* 89, 8917–8923.

Darnige, T., Figueroa-Morales, N., Bohec, P., Lindner, A. and Clément, E. (2017). Lagrangian 3D tracking of fluorescent microscopic objects in motion. *Rev. Sci. Instrum.* 88, 055106.

Dholakia, K., Drinkwater, B. W. and Ritsch-Marte, M. (2020). Comparing acoustic and optical forces for biomedical research. *Nat. Rev. Phys.* 2, 480–491.

Drescher, K., Leptos, K. C. and Goldstein, R. E. (2009). How to track protists in three dimensions. *Rev. Sci. Instrum.* 80, 014301.

Drescher, K., Goldstein, R. E., Michel, N., Polin, M. and Tuval, I. (2010). Direct measurement of the flow field around swimming microorganisms. *Phys. Rev. Lett.* 105, 168101.

Dölger, J., Nielsen, L. T., Kiørboe, T. and Andersen, A. (2017). Swimming and feeding of mixotrophic biflagellates. *Scientific Reports* 7, 39892.

Fenchel, T. (1980). Suspension Feeding in Ciliated Protozoa: Structure and Function of Feeding Organelles. *Arch. Protistenk.* 123, 239–260.

Fenchel, T. (2001). How dinoflagellates swim. *Protist* 152, 329–338.

Fortes, M. A. (1982). Axisymmetric liquid bridges between parallel plates. *Journal of Colloid and Interface Science* 88, 338–352.

Gorkov, L. P. (1962). On the forces acting on a small particle in an acoustical field in an ideal fluid. *Soviet Physics - Doklady* 6, 773–775.

Gray, J. (1955). The movement of sea-urchin spermatozoa. *J. Exp. Biol.* 32, 775–801.

Gray, J. and Hancock, G. J. (1955). The propulsion of sea-urchin spermatozoa. *J. Exp. Biol.* 32, 802–814.

Guasto, J. S., Johnson, K. A. and Gollub, J. P. (2010). Oscillatory flows induced by microorganisms swimming in two dimensions. *Phys. Rev. Lett.* 105, 168102.

Guasto, J. S., Rusconi, R. and Stocker, R. (2012). Fluid Mechanics of Planktonic Microorganisms. *Annu. Rev. Fluid Mech.* 44, 373–400.

Gutiérrez-Ramos, S., Hoyos, M. and Ruiz-Suárez, J. C. (2018). Induced clustering of *Escherichia coli* by acoustic fields. *Scientific Reports* 8, 4668.

Hammarström, B., Evander, M., Barbeau, H., Bruzelius, M., Larsson, J., Laurell, T. and Nilsson, J. (2010). Non-contact acoustic cell trapping in disposable glass capillaries. *Lab Chip* 10, 2251–2257.

Hansen, P. J. (1989). The red tide dinoflagellate *Alexandrium tamarense*: effects on behaviour and growth of a tintinnid ciliate. *Mar. Ecol. Prog. Ser.* 53, 105–116.

Joergensen, J. H. and Bruus, H. (2021). Theory of pressure acoustics with thermoviscous boundary layers and streaming in elastic cavities. *J. Acoust. Soc. Am.* 149, 3599–3610.

Kaye, G. W. C. and Laby, T. H. (1995). Tables of Physical and Chemical Constants. 16th Edition. *Longman Group Limited, UK*.

Kim, M., Huff, E., Bottier, M., Dutcher, S. K., Bayly, P. V. and Meacham, J. M. (2019). Acoustic trap-and-release for rapid assessment of cell motility. *Soft Matter* 15, 4266–4275.

Kim, M., Bayly, P. V. and Meacham, J. M. (2021). Motile cells as probes for characterizing acoustofluidic devices. *Lab on a Chip* 21, 521–533.

Lauga, E. (2020). The fluid dynamics of cell motility. *Cambridge University Press, UK*.

Laurell, T., Petersson, F. and Nilsson, A. (2007). Chip integrated strategies for acoustic separation and manipulation of cells and particles. *Chem. Soc. Rev.* 36, 492–506.

Lenshof, A., Evander, M., Laurell, T. and Nilsson, J. (2012). Acoustofluidics 5: Building microfluidic acoustic resonators. *Lab Chip* 12, 684–695.

Leão-Neto, J. P., Hoyos, M., Aider, J.-L. and Silva, G. T. (2021). Acoustic radiation force and torque on spheroidal particles in an ideal cylindrical chamber. *J. Acoust. Soc. Am.* 149, 285–295.

Lewis, N. I., Xu, W., Jericho, S. K., Kreuzer, H. J., Jericho, M. H. and Cemballa, A. D. (2006). Swimming speed of three species of *Alexandrium* (Dinophyceae) as determined by digital in-line holography. *Phycologia* 45, 61–70.

Lickert, F., Ohlin, M., Bruus, H. and Ohlsson, P. (2021). Acoustophoresis in polymer-based microfluidic devices: Modeling and experimental validation. *J. Acoust. Soc. Am.* 149, 4281–4291.

Lighthill, J. (1978). Waves in Fluids. *Cambridge University Press, UK*.

Manneberg, O., Vanherberghen, B., Önfelt, B. and Wiklund, M. (2009). Flow-free transport of cells in microchannels by frequency-modulated ultrasound. *Lab on a Chip* 9, 833–837.

Muller, P. B. and Bruus, H. (2015). Theoretical study of time-dependent, ultrasound-induced acoustic streaming in microchannels. *Phys. Rev. E* 92, 063018.

Purcell, E. M. (1977). Life at low Reynolds number. *American Journal of Physics* 45, 3–11.

Rode, M., Kiørboe, T. and Andersen, A. (2022). Feeding flow and membranelle filtration in ciliates. *Physical Review Fluids* 7, 023102.

Saito, M., Izumida, S. and Hirota, J. (1997). Ultrasonic trapping of paramecia and estimation of their locomotive force. *Appl. Phys. Lett.* 71, 1909–1911.

Saito, M., Kitamura, N. and Terauchi, M. (2002). Ultrasonic manipulation of locomotive microorganisms and evaluation of their activity. *Journal of Applied Physics* 92, 7581–7586.

Saito, M. and Morita, S. (2006). Ultrasonic and spectroscopic studies on photoactivation of euglena. *Journal of Applied Physics* 100, 114701.

Skov, N. R., Bach, J. S., Winckelmann, B. G. and Bruus, H. (2019). 3D modeling of acoustofluidics in a liquid-filled cavity including streaming, viscous boundary layers, surrounding solids, and a piezoelectric transducer. *AIMS Mathematics* 4, 99–111.

Takatori, S. C., De Dier, R., Vermant, J. and Brady, J. F. (2016). Acoustic trapping of active matter. *Nature Communications* 7, 10694.

Thalhammer, G., Steiger, R., Bernet, S. and Ritsch-Marte, M. (2011). Optical macro-tweezers: trapping of highly motile micro-organisms. *J. Opt.* 13, 044024.

Wei, D., Dehnavi, P. G., Aubin-Tam, M.-E. and Tam, D. (2019). Is the Zero Reynolds Number Approximation Valid for Ciliary Flows? *Phys. Rev. Lett.* 122, 124502.